Coulomb correlation effects in semiconductor quantum dots: The role of dimensionality

Coulomb correlation effects in semiconductor quantum dots: The role of dimensionality

Massimo Rontani, Fausto Rossi, Franca Manghi, and Elisa Molinari
Istituto Nazionale per la Fisica della Materia (INFM), and Dipartimento di Fisica, Università di Modena, via Campi 213/A, I-41100 Modena, Italy

(Received 27 August 1998)

We study the energy spectra of small three-dimensional (3D) and two-dimensional (2D) semiconductor quantum dots through different theoretical approaches (single-site Hubbard and Hartree-Fock Hamiltonians); in the smallest dots we also compare with exact results. We find that purely 2D models often lead to an inadequate description of the Coulomb interaction existing in realistic structures, as a consequence of the overestimated carrier localization. We show that the dimensionality of the dots has a crucial impact on (i) the accuracy of the predicted addition spectra, and (ii) the range of validity of approximate theoretical schemes. When applied to realistic 3D geometries, the latter are found to be much more accurate than in the corresponding 2D cases for a large class of quantum dots; the single-site Hubbard Hamiltonian is shown to provide a very effective and accurate scheme to describe quantum dot spectra, leading to good agreement with experiments. [S0163-1829(99)10211-X]

I. INTRODUCTION

Adding an electron into a semiconductor quantum dot (QD) produces a variation in the energy of the system that depends on single-particle quantum confinement as well as on the Coulomb interaction between carriers.[1] Understanding such *addition-energy* is a key step toward controlling the physics of single-electron devices. At the same time, the addition spectra of quantum dots offer a unique probe of few-particle interactions in regimes that are not experimentally accessible in atomic physics. The experimental effort in this direction developed very rapidly after the recent fabrication of controlled small-QD devices based on gated vertical heterostructures[2] or self-assembled dots.[3] The resulting addition spectra show a clear shell structure, corresponding to the symmetries of the confining potential, with a filling sequence analogous to Hund's rule in atomic physics.

From the theoretical point of view, a general interpretation of these features was obtained by calculating the energy spectrum for a strictly two-dimensional (2D) quantum dot, and using either exact methods (for very few electrons), or approximate—usually Hartree-Fock—methods.[4] The assumption of a purely 2D model was initially motivated by the typical disklike shape of the QD potential, whose extension along z is (slightly) smaller than the lateral extension of the carrier ground state in the xy plane. If one adopts a separable picture for the QD confining potential, $V=V(z)+V(x,y)$, the relevant (i.e., lowest) single-electron states can be all associated to the ground state of $V(z)$. From the point of view of single-particle states the 2D assumption is therefore justified.

In view of the three-dimensional (3D) nature of the Coulomb interaction, however, the 2D model introduces additional approximations in the calculation of the Coulomb integrals, which are sensitive to the spatial extension—2D vs 3D—of the single-particle wave functions.[5,6] In turn, Coulomb integrals control electron-electron correlation, and influence the quantitative determination of addition spectra and their dependence on magnetic field. At the same time, the strength of the Coulomb interaction is also the key parameter determining the accuracy and range of validity of the approximations which must be introduced for dots with many electrons.

In this paper we investigate theoretically the addition spectra of realistic QD structures, with special emphasis on the effects of electron-electron repulsion and their dependence on the geometry and dimensionality of the confining potential. In Sec. II, we compare different approximate solutions of the general Hamiltonian for N interacting electrons confined in a QD structure; in particular we consider the single-site Hubbard (SSH) scheme introduced in Ref. 5, and the standard Hartree-Fock (HF) method.

In Sec. III, we focus on the simplest case, i.e., a two-electron system within a parabolic confining potential, and calculate the exact energy eigenvalues and pair-correlation functions for the 2D and 3D cases. As in Ref. 7, we use this prototypical system—called artificial or QD helium—as a reference to evaluate the accuracy of the different approximation schemes: We find that both the importance of corrections beyond the HF scheme, and the differences between HF and SSH schemes, are drastically reduced for a realistic 3D description of the dot with respect to its 2D modelization, mainly as a consequence of the reduced Coulomb integrals. This suggests the reliability of a fully 3D mean-field treatment of semiconductor QD's.

Section IV is then devoted to the application of HF and SSH methods to 3D and 2D quantum dots with a larger number of electrons. We compare both methods for QD structures of different geometries, and demonstrate that SSH is an accurate and efficient scheme for realistic, i.e., 3D-like, dots. Finally, we discuss the implications of our results for the interpretation of recent experimental data vs magnetic field in QD structures, and draw some conclusions.

II. THEORETICAL APPROACH: EXACT FORMULATION AND APPROXIMATION SCHEMES

Our aim is to describe N electrons, confined in a QD structure (with harmonic in-plane confining potential) and

interacting via Coulomb law, possibly in the presence of an external magnetic field perpendicular to the plane. The general N-particle Hamiltonian is

$$\hat{\mathcal{H}}=\sum_{i=1}^{N}\hat{H}_0(i)+\tfrac{1}{2}\sum_{i\neq j}\frac{e^2}{\kappa|\boldsymbol{r}_i-\boldsymbol{r}_j|}, \tag{1}$$

where the single-particle Hamiltonian, within the effective-mass approximation, is

$$\hat{H}_0(i)=\frac{1}{2m^*}\left(\hat{\boldsymbol{p}}+\frac{e}{c}\hat{\boldsymbol{A}}(\boldsymbol{r}_i)\right)^2+\frac{1}{2}m^*\omega_0^2(x_i^2+y_i^2)+V(z_i). \tag{2}$$

Here $\hat{\boldsymbol{A}}$ is the vector potential, κ and m^* are the scalar dielectric constant and the effective electron mass in the semiconductor, ω_0 is the characteristic oscillator frequency of the in-plane confining potential, and $V(z)$ is the confining potential along z; $V(z)$ can be chosen either as a harmonic potential [$V(z)=\frac{1}{2}m^*\omega_0^2z^2$], a square well, or a zero-width infinite barrier to describe spherical, cylindrical, or disk-shaped QD structures, respectively. Here Zeeman coupling between spin and magnetic field has been neglected.

This general Hamiltonian can be written in second quantized form on the complete and orthonormalized basis of single particle states

$$\hat{\mathcal{H}}=\sum_{\alpha\sigma}\varepsilon_\alpha\hat{c}^\dagger_{\alpha\sigma}\hat{c}_{\alpha\sigma}+\tfrac{1}{2}\sum_{\alpha\beta\gamma\delta}\sum_{\sigma\sigma'}V_{\alpha\sigma,\beta\sigma';\gamma\sigma',\delta\sigma}\hat{c}^\dagger_{\alpha\sigma}\hat{c}^\dagger_{\beta\sigma'}\hat{c}_{\gamma\sigma'}\hat{c}_{\delta\sigma}. \tag{3}$$

Here ε_α are the eigenenergies of the one-particle Hamiltonian $\hat{H}_0$; $\hat{c}^\dagger_{\alpha\sigma}$ and $\hat{c}_{\alpha\sigma}$ the creation and destruction operators for an electron with orbital index α and spin σ; and $V_{\alpha\sigma,\beta\sigma';\gamma\sigma',\delta\sigma}$ are the two-body matrix elements of the electron-electron interaction

$$V_{\alpha\sigma,\beta\sigma';\gamma\sigma',\delta\sigma}=\sum_{ss'}\int\phi^*_{\alpha\sigma}(\boldsymbol{r},s)\phi^*_{\beta\sigma'}(\boldsymbol{r}',s')\times\frac{e^2}{|\boldsymbol{r}-\boldsymbol{r}'|}\phi_{\gamma\sigma'}(\boldsymbol{r}',s')\phi_{\delta\sigma}(\boldsymbol{r},s)d\boldsymbol{r}\,d\boldsymbol{r}'$$

where $\phi_{\alpha\sigma}(\boldsymbol{r},s)=\phi_\alpha(\boldsymbol{r})\chi_\sigma(s)$ are the single-particle eigenfunctions.

It is useful to isolate, among the Coulomb matrix elements, the ''semidiagonal'' ones, namely,

$$V_{\alpha\sigma,\beta\sigma;\beta\sigma,\alpha\sigma}=V_{\alpha\sigma,\beta-\sigma;\beta-\sigma,\alpha\sigma}\equiv U_{\alpha\beta},$$

$$V_{\alpha\sigma,\beta\sigma;\alpha\sigma,\beta\sigma}\equiv J_{\alpha\beta}.$$

These are the usual direct and exchange integrals which can be written more explicitly as

$$U_{\alpha\beta}=e^2\int\int\frac{|\phi_\alpha(\boldsymbol{r})|^2|\phi_\beta(\boldsymbol{r}')|^2}{\kappa|\boldsymbol{r}-\boldsymbol{r}'|}d\boldsymbol{r}\,d\boldsymbol{r}', \tag{4}$$

$$J_{\alpha\beta}=e^2\int\int\frac{\phi^*_\alpha(\boldsymbol{r})\phi^*_\beta(\boldsymbol{r}')\phi_\alpha(\boldsymbol{r}')\phi_\beta(\boldsymbol{r})}{\kappa|\boldsymbol{r}-\boldsymbol{r}'|}d\boldsymbol{r}\,d\boldsymbol{r}'. \tag{5}$$

In this way, Eq. (2) becomes

$$\hat{\mathcal{H}}=\hat{\mathcal{H}}^{\mathrm{SSH}}+\tfrac{1}{2}{\sum_{\alpha\beta\gamma\delta}}'\sum_{\sigma\sigma'}V_{\alpha\sigma,\beta\sigma';\gamma\sigma',\delta\sigma}\hat{c}^\dagger_{\alpha\sigma}\hat{c}^\dagger_{\beta\sigma'}\hat{c}_{\gamma\sigma'}\hat{c}_{\delta\sigma}; \tag{6}$$

where the prime on the first summation is to omit the terms with $\alpha=\delta,\beta=\gamma$ and $\alpha=\gamma,\beta=\delta$ and

$$\hat{\mathcal{H}}^{\mathrm{SSH}}=\sum_{\alpha\sigma}\varepsilon_\alpha\hat{n}_{\alpha\sigma}+\tfrac{1}{2}\sum_{\alpha\beta\sigma}[(U_{\alpha\beta}-J_{\alpha\beta})\hat{n}_{\alpha\sigma}\hat{n}_{\beta\sigma}+U_{\alpha\beta}\hat{n}_{\alpha\sigma}\hat{n}_{\beta-\sigma}]. \tag{7}$$

The relevance of this formal partition is twofold: (i) it naturally leads to a perturbation expansion in the off-diagonal interactions which are in general smaller than the semidiagonal ones; (ii) moreover, the *unperturbed* term $\hat{\mathcal{H}}^{\mathrm{SSH}}$ is one-body-like, with single Slater determinants as *exact* eigenstates. The SSH approach defined in Ref. 5 consists of assuming that $\hat{\mathcal{H}}\simeq\hat{\mathcal{H}}^{\mathrm{SSH}}$, which amounts to neglecting the second- and higher-order contributions in the off-diagonal interactions, the first-order one being exactly zero.

The assumption that the off-diagonal $V_{\alpha,\beta;\gamma,\delta}$ are negligible with respect to the semidiagonal ones is implicit in all the methods which describe electron correlation in terms of the Hubbard model, either in its original form,[8] including only on-site interaction between opposite spin electrons, proportional to $U_{\alpha\beta}$, or adding the interaction between parallel spin electrons as well, proportional to $(U_{\alpha\beta}-J_{\alpha\beta})$. The important point here is that when the Hubbard model is applied to an isolated QD, i.e., to a single site, the Hubbard Hamiltonian turns out to be one-particle-like: this is so because the intersite hopping of the traditional Hubbard Hamiltonian is absent in this case and the commutator $[\hat{\mathcal{H}}^{\mathrm{SSH}},\hat{n}_{\alpha\sigma}]$ is zero. As a consequence, the Slater determinants, eigenstates of the single-particle Hamiltonian $\hat{H}_0$, are exact eigenstates of $\hat{\mathcal{H}}^{\mathrm{SSH}}$ as well.

Within the SSH approach the total energy of N electrons in a QD structure is given by

$$E^{\mathrm{SSH}}(N)=\langle\Phi^N|\hat{\mathcal{H}}^{\mathrm{SSH}}|\Phi^N\rangle=\sum_{\alpha\sigma}\varepsilon_\alpha\langle\hat{n}_{\alpha\sigma}\rangle+\tfrac{1}{2}\sum_{\alpha\beta\sigma}[U_{\alpha\beta}\langle\hat{n}_{\beta-\sigma}\rangle+(U_{\alpha\beta}-J_{\alpha\beta})\langle\hat{n}_{\beta\sigma}\rangle]\langle\hat{n}_{\alpha\sigma}\rangle, \tag{8}$$

where $|\Phi^N\rangle$ is a Slater determinant eigenvector of $\hat{H}_0$, and $\langle\,\rangle$ denotes the average over the many-particle eigenstate, which in our case simply reduces to the orbital occupation number.

The proposed SSH approach shares in common with Hartree-Fock methods the form of the total energy, which in both schemes is expressed as the average of the exact Hamiltonian over a single Slater determinant; the variational

prescription—allowing for the construction of optimal single-particle orbitals through the self-consistent solution of a single-particle eigenvalue problem—is not present in the SSH approach. We notice, however, that the importance of self-consistency is strongly related to the relative weight of Coulomb matrix elements: the HF potential entering the self-consistent HF one-particle Hamiltonian is in fact related to the direct and exchange Coulomb integrals; similarly, the SSH approximation is exact—without any need of self-consistency—whenever the higher-order contributions from the off-diagonal Coulomb matrix elements are negligible. For this reason we expect that a lower localization of the confined single-particle states in three dimensions with respect to two dimensions, giving rise to smaller nondiagonal Coulomb integrals, will reduce the difference between HF and SSH results. To check this point in detail, we have explicitly performed HF calculations; we have used in particular the matrix form of the unrestricted HF equation.[9]

Whenever possible, it is obviously useful to compare the outcomes of different approximate schemes with exact results. This is done in Sec. III, where we consider the exactly solvable two-electron QD (artificial helium) in different confinement regimes; we will show that the differences between HF and SSH results will be always comparable with those between HF and exact results, and that they scale with the dimensionality of the confining potential.

III. TWO-ELECTRON PROBLEM

In this section we will study the motion of two electrons within a QD structure in two and three dimensions. In this case, the exact Hamiltonian (1) reduces to

$$\hat{\mathcal{H}}=\hat{H}_0(1)+\hat{H}_0(2)+\frac{e^2}{\kappa|\boldsymbol{r}_1-\boldsymbol{r}_2|}. \tag{9}$$

Here $\boldsymbol{r}_i$ is the position of the electron, $\boldsymbol{r}_i\equiv(x_i,y_i)$ in two dimensions or $\boldsymbol{r}_i\equiv(x_i,y_i,z_i)$ in three dimensions, and $\boldsymbol{p}_i$ the corresponding momentum.

To solve this equation, we perform the standard transformation[10] to center of mass (CM) coordinates, $\boldsymbol{R}=(\boldsymbol{r}_1+\boldsymbol{r}_2)/2$, $\hat{\boldsymbol{P}}=\hat{\boldsymbol{p}}_1+\hat{\boldsymbol{p}}_2$, and relative-motion (rm) coordinates, $\boldsymbol{r}=\boldsymbol{r}_1-\boldsymbol{r}_2$, $\hat{\boldsymbol{p}}=(\hat{\boldsymbol{p}}_1-\hat{\boldsymbol{p}}_2)/2$. The two-body Hamiltonian thus splits into CM and rm parts:

$$\hat{\mathcal{H}}=\hat{H}_{\rm CM}+\hat{H}_{\rm rm}, \tag{10}$$

where

$$\hat{H}_{\rm CM}=\frac{\hat{\boldsymbol{P}}^2}{2M}+\frac{1}{2}M\omega^2R^2, \tag{11}$$

$$\hat{H}_{\rm rm}=\frac{\hat{\boldsymbol{p}}^2}{2\mu}+\frac{1}{2}\mu\omega^2r^2+\frac{e^2}{\kappa r}, \tag{12}$$

with $M=2m^*$, and $\mu=m^*/2$. The CM Hamiltonian $\hat{H}_{\rm CM}$ has the form of a simple harmonic oscillator. For the rm Hamiltonian $\hat{H}_{\rm rm}$, it is easy to separate variables and obtain a radial differential equation, which gives solutions with the same set of quantum numbers as for the harmonic oscillator. Solutions and notations for the 2D and 3D cases are summarized in Appendix A for both $\hat{H}_{\rm CM}$ and $\hat{H}_{\rm rm}$.

By denoting the CM and rm quantum numbers with capital and small letters, respectively, the eigenvalues for the two-particle system can be written as

$$E_{NM,nm}=\hbar\omega(2N+|M|+1)+\epsilon_{nm} \tag{13}$$

in the 2D case, and

$$E_{NL,nl}=\hbar\omega\left(2N+L+\frac{3}{2}\right)+\epsilon_{nl} \tag{14}$$

in the 3D spherical case, the cylindrical 3D helium QD reducing to an effective 2D one (see Appendix A). Here ϵ_{nm} and ϵ_{nl} are the rm eigenvalues in two and three dimensions, respectively. Note that degeneracy is strongly reduced by Coulomb interaction with respect to the noninteracting case.

The corresponding two-particle total eigenfunctions are

$$\Psi_{NM,nm;SS_z}(\boldsymbol{r}_1,s_1;\boldsymbol{r}_2,s_2)=\Phi_{NM}(\boldsymbol{R})\varphi_{nm}(\boldsymbol{r})\chi(S,S_z) \tag{15}$$

for 2D and 3D cylinders, and

$$\Psi_{NLM_z,nlm_z;SS_z}(\boldsymbol{r}_1,s_1;\boldsymbol{r}_2,s_2)=\Phi_{NLM_z}(\boldsymbol{R})\varphi_{nlm_z}(\boldsymbol{r})\chi(S,S_z) \tag{16}$$

for a 3D sphere. Here $\Phi(\boldsymbol{R})$ and $\varphi(\boldsymbol{r})$ are the spatial CM and rm eigenfunctions, respectively, and $\chi(S,S_z)$ is the spin function of a state with total spin $\hbar^2S(S+1)$ and z projection S_z. Note that the parity of the rm spatial eigenfunction is defined (total orbital angular momentum and spin are conserved) and connected with the value of total spin by the antisymmetry of the two-particle total wave function $\Psi(\boldsymbol{r}_1,s_1;\boldsymbol{r}_2,s_2)$. For both the disk and the cylinder, this implies that if m is even, the state is a singlet ($S=0$), and, if m is odd, the state is a triplet ($S=1$). Similarly for the sphere case, if l is even, the state is a singlet ($S=0$), and if l is odd, the state is a triplet ($S=1$).

In the above eigenvalues and eigenfunctions of the two-electron dot, the ingredients related to the CM Hamiltonian are known analytically (see Appendix A), while the rm energies and wave functions must be determined numerically. This is done by exact diagonalization of the rm eigenvalue problem (Appendix A), thereby yielding the full 2D and 3D spectrum of the QD helium.

Before comparing these exact results with the SSH approach, we point out that Hamiltonian (9) can be translated into a second-quantized form; this is done in terms of the same quantum numbers using CM and rm variables. The two-particle Hilbert space is the Kronecker product of the CM and rm single-particle spaces, generated, respectively, by the basis $\{|N\rangle\}_N$ (with eigenvalues E_N and creation operators $\hat{a}_N^\dagger$) and $\{|n\rangle\}_n$ (with eigenvalues ϵ_n and creation operators $\hat{a}_n^\dagger$). Here, for simplicity, N and n label the whole set of CM and rm quantum numbers, respectively. The second-quantized form of the two-particle Hamiltonian $\hat{\mathcal{H}}$, in this variable, is then given by

$$\hat{\mathcal{H}}=\sum_N E_N\hat{a}_N^\dagger\hat{a}_N+\sum_n \epsilon_n\hat{a}_n^\dagger\hat{a}_n+\sum_{nn'} V_{nn'}\hat{a}_n^\dagger\hat{a}_{n'}. \tag{17}$$

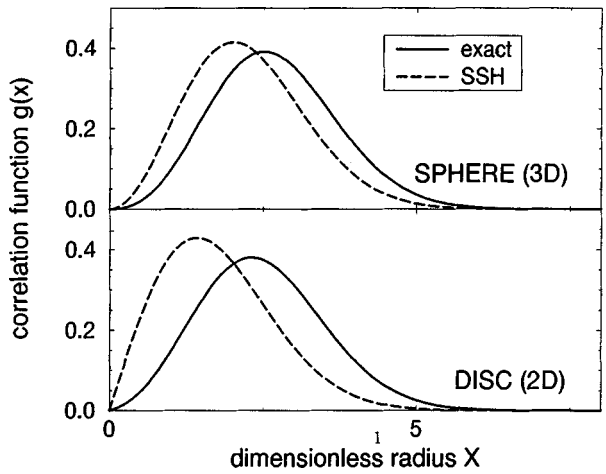

FIG. 1. Ground-state spatial pair-correlation function $g(x)$ for 3D (spherical) and 2D two-electron QD's: exact and SSH results are reported. Here $x=(2m^*\omega_0 r^2/\hbar)^{1/2}$ is the dimensionless relative radial coordinate and $g(x)$ is normalized in such a way that $\int_0^\infty g(x)dx=1$. The in-plane confinement energy is $\hbar\omega_0=5$ meV.

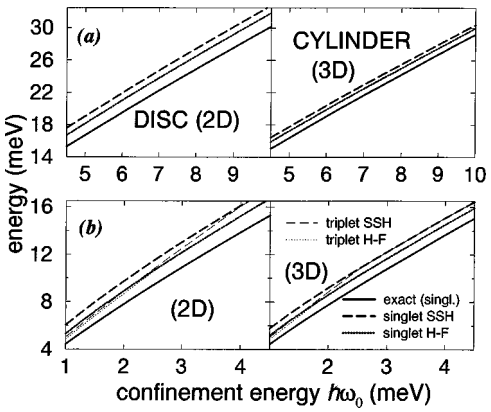

FIG. 2. (a) Ground-state energy of the artificial He QD as a function of the confinement energy $\hbar\omega_0$, calculated within different approaches (exact, SSH, and HF). The range of $\hbar\omega_0$ is 4.5–10 meV. The two panels correspond to 2D and 3D (cylindrical) geometries. The ground-state configuration is always a spin singlet. (b) Spin-singlet (spin-triplet) energies vs confinement energies $\hbar\omega_0$. The range of $\hbar\omega_0$ is 1–4.5 meV. The two panels are relative to 2D and 3D (cylindrical) geometries. The exact ground state is always a singlet, while a singlet-triplet crossover occurs for both approximated schemes in the low-energy region.

This formulation allows us to obtain the result of the previously discussed Hubbard model, by simply neglecting all off-diagonal matrix elements in Eq. (17):

$$\hat{\mathcal{H}}^{\mathrm{SSH}}=\sum_N E_N\hat{a}_N^\dagger\hat{a}_N+\sum_n(\epsilon_n+V_{nn})\hat{a}_n^\dagger\hat{a}_n, \qquad (18)$$

i.e., manifestly the noninteracting Hamiltonian ''renormalized'' by Coulomb interaction.

In order to check the reliability of the approximations and the role of dimensionality of the confining potential, we have calculated ground-state properties for QD's with different confinement energies, i.e., different values of $\hbar\omega_0$, assuming either a 2D or 3D confining potential. The quality of the ground-state eigenfunctions can be probed by the spatial pair correlation function $f(\boldsymbol{r})$:

$$f(\boldsymbol{r})=K\left\langle\sum_{i\neq j}\delta(\boldsymbol{r}-\boldsymbol{r}_i+\boldsymbol{r}_j)\right\rangle. \qquad (19)$$

Because of the circular symmetry, $f(\boldsymbol{r})$ depends only on the modulus of the relative distance $\boldsymbol{r}$. Here, the factor K is chosen in such a way that, if we define the dimensionless relative distance $x=r\sqrt{2m^*\omega_0/\hbar}$, the quantity $g(x)=xf(x)$ for the 2D and 3D cylinder cases, and $g(x)=x^2f(x)$ for a 3D sphere is normalized:

$$\int_0^\infty g(x)dx=1.$$

We have calculated this quantity both exactly and according to the SSH scheme for an in-plane confining energy $\hbar\omega_0=5$ meV (throughout the paper we use $m^*=0.065m_e$ inside the dot and $m^*=0.079m_e$ outside; $\kappa=12.98$, as in the QD of Ref. 2; and m_e is the electronic mass); the results are shown in Fig. 1. The deviations between SSH and exact results clearly depend on the dimensionality of the confining potential: in disk-shaped 2D QD's the SSH approximation is found to overestimate the probability of finding the two electrons close together, in analogy with HF results[7]; the differences between exact and SSH results are significantly reduced assuming a 3D confining potential. This result is coherent with what is found for other ground-state properties: Fig. 2(a) shows the ground-state energies calculated for dots with different confinement energies, $\hbar\omega_0$, in the range between 4.5 and 10 meV. We compare the exact results with the outcomes of HF and SSH calculations assuming 2D and 3D confinement potentials. Notice that the differences between HF and SSH are always smaller—by approximately 50%—than the corresponding differences with respect to the exact results; moreover the 3D confinement reduces the overall deviation of both HF and SSH by about 60%.

Since the SSH scheme is exact at the first perturbative order in the off-diagonal matrix elements of the e-e interaction, it is interesting to check the importance of the next perturbative corrections. Details of how the perturbative expansion is actually performed for the helium QD are reported in Appendix B. Figure 3 reports exact and SSH ground-state energies compared with the results of second-order perturbation theory, showing that second-order corrections become much smaller if a 3D confinement is assumed.

The situation becomes more complicated when considering dots with smaller confinement energies: in this case the HF and SSH differ from the exact result not only quantitatively but also qualitatively, predicting the two-particle ground state to be a triplet instead of a singlet, as it should be. This is shown in Fig. 2(b), where again the exact HF and SSH results are shown for dots of different confinement energies. The difference between triplet- and singlet-state energies decreases with increasing confinement energy both for SSH and HF approximations until a crossover occurs; assuming a 3D confining potential, the confinement energy of this crossover is reduced, and this again is true both for SSH and HF approximations.

We may summarize this analysis on helium QD by concluding that the assumed 3D confinement potential reduces the differences between approximate (SSH and HF) solutions

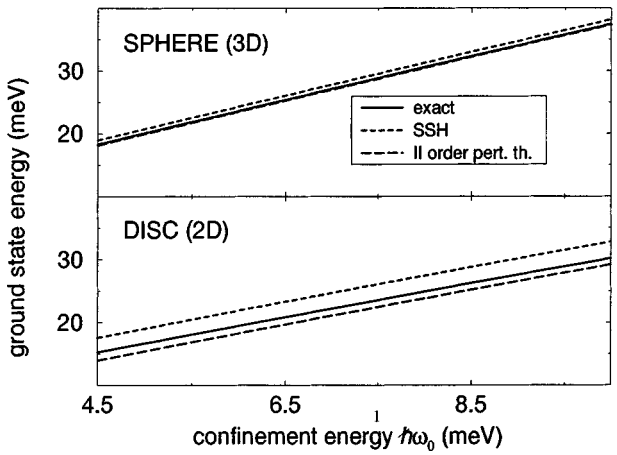

FIG. 3. Ground-state energy of the artificial He QD as a function of the confinement energy $\hbar\omega_0$, as obtained via exact diagonalization, SSH approximation scheme, and Rayleigh-Schrödinger perturbation theory at the second order in the off-diagonal Coulomb matrix elements. Both 3D (spherical) and 2D cases are shown.

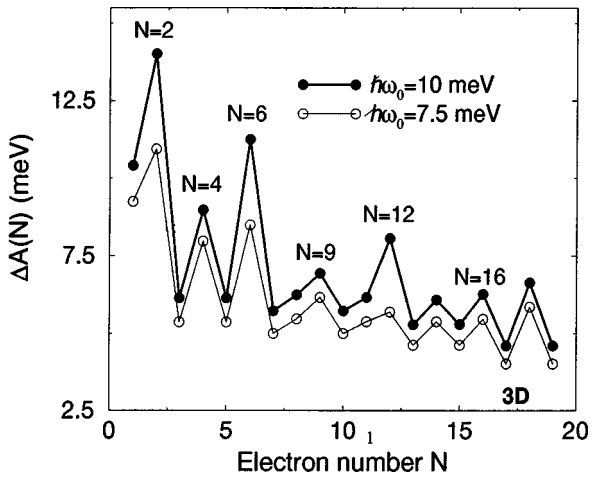

FIG. 4. Calculated SSH addition-energy increment ΔA as a function of the total number N of electrons for two different QD structures, both characterized by a parabolic potential in the xy plane (confining energy $\hbar\omega_0$) and by a finite-barrier quantum-well potential along the z direction (3D cylindrical model).

with respect to the exact ones, both in terms of ground-state eigenfunctions and eigenenergies.

IV. MANY-ELECTRON PROBLEM

The key quantity that characterizes single-electron transport into a QD is the addition energy, i.e., the energy $A(N)$ required to place an extra electron into a dot that is initially occupied by $N-1$ electrons. Such a quantity, analogous to electron affinity in atomic physics, can be measured experimentally as a function of N. It has been shown[2] that the measured voltage increment ΔA between successive single-electron tunneling processes—i.e., between two successive maxima in the conductance—peaks at ''magic'' values of N corresponding to the filling of complete shells ($N=2$, 6, and 12), as well as to half-shell filling (e.g., $N=4$). The existence of these half-shell filling features is reminiscent of Hund's rule in atomic physics,[2,11,12] and is intimately related to electron-electron interaction.

The results of SSH theory for the addition-energy variations, $\Delta A(N)=A(N+1)-A(N)$, are displayed in Fig. 4 as a function of the electron number N for two different 3D cylindrical quantum dots. Here $A(N)$ is obtained as $E^{\mathrm{SSH}}(N)-E^{\mathrm{SSH}}(N-1)$, where $E^{\mathrm{SSH}}(N)$ is the ground-state energy in Eq. (8). As we can see, $\Delta A(N)$ exhibits peaks corresponding both to complete and half-shell filling, thus well reproducing the experimental evidence in Ref. 2. This behavior is the result of the interplay between single-particle contributions and electron-electron repulsion: the single-particle term favors complete shell filling, while the repulsion among parallel-spin electrons, smaller than the repulsion among opposite-spin ones, makes the configurations with maximum total spin energetically favored (Hund's rule). This is the physical origin of the half-shell-filling structure: indeed, adding an electron to a half-filled shell forces the double occupancy of a level; consequently, ΔA is raised by the dominant Coulomb repulsion $U_{\alpha\alpha}$ between opposite-spin electrons on the same level.

For some nonclosed shell configurations the total spin turns out to be not determined by Hund's rule: in particular, for $N=16$ we find a ground state with total spin $S=0$. Similar deviations from Hund's rule have been found for large electron numbers ($N>20$) and associated with spin-density-wave instabilities; for smaller numbers ($N=16$ and 18) the same $S=0$ spin-density-wave state has been found to be a low-energy ''spin isomer,'' slightly higher in energy than the ground-state configuration.[13]

From our calculations we may say that the $S=0$ configuration in dots with large N may be favored by the reduced repulsion between electrons in high shells: in the fourth shell, for instance, the Coulomb integrals $U_{\alpha\beta}$ relative to orbitals with higher values of the orbital momentum may be smaller than the corresponding terms relating two levels with smaller angular momentum; the double occupation of an orbital with high orbital momentum m (i.e., the level with $n=0$, $m=3$; see Appendix A for the notation) with antiparallel-spin electrons may therefore cost less than having parallel-spin electrons on different degenerate orbitals, but with smaller m (i.e., the levels $n=1$ and $m=1$). The same interplay also explains the peaks in $\Delta A(N)$ for $N=14$ and 18.[14]

We want to stress that also in the case of many electrons the reliability of the results of SSH approach is comparable with HF ones. The explicit comparison between the addition energy variation calculated according to SSH and HF schemes and for 2D and 3D confinements is reported in Fig. 5, showing that ΔA always peaks at the same electron numbers, and that the agreement between SSH and HF results improves on going from the 2D to the 3D confinement model.

Ground-state configurations and filling rules change when a magnetic field is applied. It affects both single-particle energies and Coulomb and exchange integrals through the induced changes in the wave-function localization. Figure 6 shows the U and J integrals vs B for the first states, obtained for $\hbar\omega_0=7.5$ meV. For comparison, we also show the corresponding quantities calculated within a strictly 2D confinement model. We can see that U integrals describing the interaction between opposite-spin electrons are a few meV

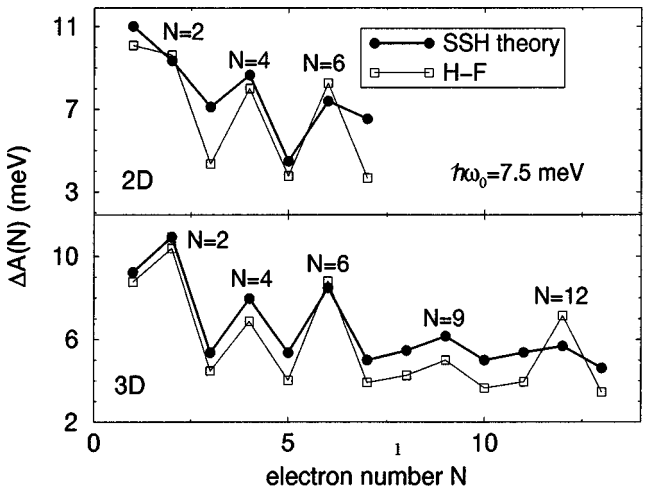

FIG. 5. Comparison between SSH and HF addition-energy increments ΔA as a function of the total number N of electrons in the dot. Here the upper panel corresponds to the 2D geometry, while the lower one corresponds to the 3D cylindrical model. The in-plane confinement energy is $\hbar\omega_0 = 7.5$ meV.

smaller in the case of 3D confinement, while the differences in the interaction between parallel-spin ones are much smaller. This is going to affect dramatically the energy balance which determines ground-state configurations, thus clearly showing the failure of a pure 2D description of state-of-the-art QD structures.

As already mentioned, according to the SSH approach the off-diagonal matrix elements of the electron-electron interaction are assumed to be negligible. In Fig. 6 the values of two of them are reported as functions of the applied magnetic field. As expected, we clearly see that for any B value they are negligible compared to all the other semidiagonal contributions, and even more so in three dimensions with respect to the 2D case.

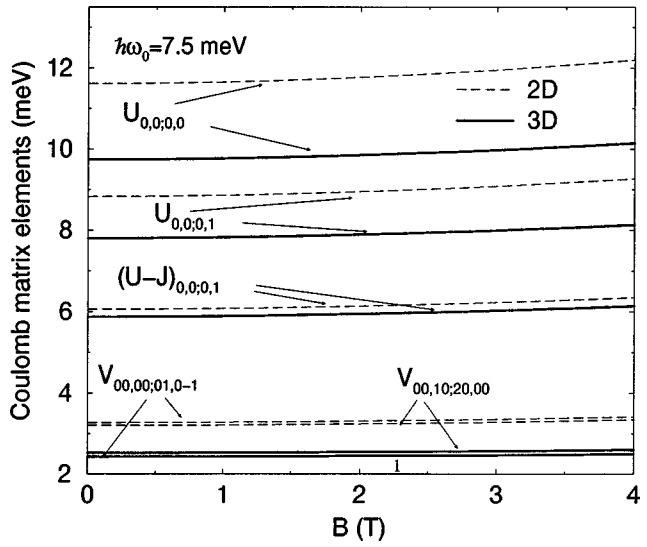

FIG. 6. Coulomb ($U_{\alpha;\beta}$) and exchange ($J_{\alpha;\beta}$) integrals as well as off-diagonal Coulomb matrix elements ($V_{\alpha,\beta;\gamma,\delta}$), as functions of the magnetic field B for both 2D and 3D cases. Here α and β denote the sets of radial and angular quantum numbers (n,m) for the various single-particle states involved in the two-body interaction process. The in-plane confinement energy is $\hbar\omega_0 = 7.5$ meV.

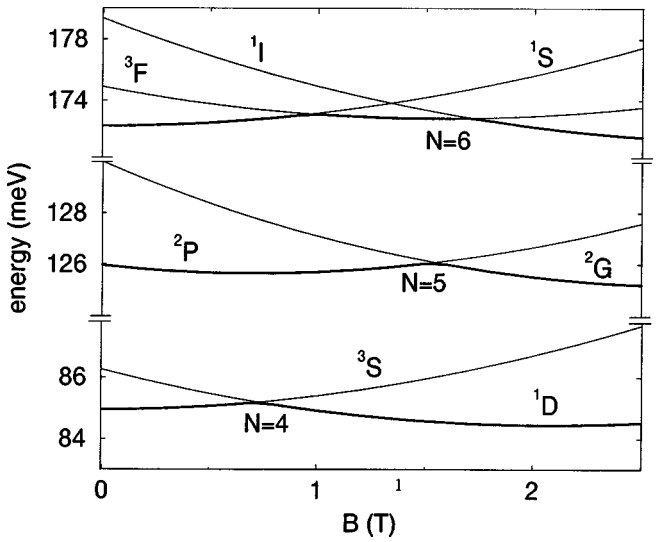

FIG. 7. Total energy E^{SSH} as a function of the applied magnetic field B corresponding to N electrons in a dot with confinement energy $\hbar\omega_0 = 7.5$ meV. For any given value of N, all the possible configurations, denoted by the usual atomic physics terms ^{2S+1}L, have been considered.

Figure 7 shows the total energy E^{SSH} as a function of the applied magnetic field B for different values of the electron number N in a dot with confinement energy $\hbar\omega_0 = 7.5$ meV. It appears that for sufficiently large values of B the Hamiltonian term linear in the magnetic field becomes dominant, making configurations with higher total angular quantum number energetically favorable. This is also the physical origin of the wiggles in the $A(N)$ vs B plot shown in Fig. 8 and observed in the experiments reported in Ref. 2.

Other authors have explicitly considered the question of dimensionality in theoretical modelization of semiconductor QD's. Kumar, Laux, and Stern[15] self-consistently computed the one-particle confining potential in a square QD. Accord-

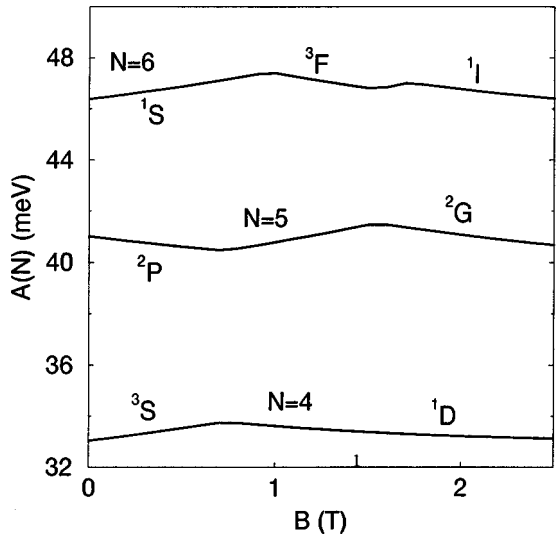

FIG. 8. Addition energy $A(N)$ as a function of the magnetic field B calculated for a realistic (3D) QD structure with confinement energy $\hbar\omega_0 = 7.5$ meV and for different values of N. The labels indicate the electronic terms for the ground-state configurations, that depend on B.

ing to their results, our assumption of an in-plane parabolic confining potential plus a well in the perpendicular direction is seen to be quite reliable and general, as well as the *ansatz* of considering only the ground-state motion along z, at least for few electron dots. Steinebach *et al.*[16] pointed out the importance of a full 3D model to treat spin-density excitations (SDE's) in semiconductor wires and dots. Specifically, they used the analogous of Eq. (A4) as an effective 3D Coulomb interaction, and they found that a 2D description artificially enhances the interaction strength and is unable to predict experimental Raman spectra. The necessity of a 3D modelization is then seen to emerge not only in the description of ground-state and single-particle processes, like addition spectra, but also in two-particle processes, like SDE's.

V. SUMMARY AND CONCLUSIONS

We have presented a theoretical investigation of Coulomb-correlation effects in semiconductor quantum dots. In particular, we have performed a detailed analysis of the addition-spectrum problem for few-electron quantum-dot structures (macroatoms), pointing out possible analogies with more conventional Coulomb-correlation effects in atomic physics.

Our primary goal was to understand to which extent the various approximation schemes, such as Hartree-Fock or Hubbard models, are able to properly describe Coulomb correlation in realistic, state-of-the-art QD's. To this end, we have first compared approximate results to the exact solution for the prototypical case of a two-electron system, the so-called quantum-dot helium; we have repeated such analysis for different dimensionalities, considering 3D (spherical and cylindrical geometry) and pure 2D structures. The main result is that the degree of accuracy of any approximation scheme depends strongly on the dimensionality of the problem. More specifically, the pure 2D model—often used for a description of quantum dots—is found to give approximate results which differ significantly from the exact solution. We have demonstrated that this is not a general failure of the approximation scheme, but that it rather reflects a pathological behavior originating from the unphysical nature of the pure 2D model. Indeed, for the case of a 3D cylindrical model—which provides a much better description of realistic QD structures—the difference between an exact solution and approximate results is found to be much smaller, thus confirming the validity of the various approximation schemes considered.

The same analysis has been then extended to many-electron systems for which addition-spectra measurements are available. Using different approximation schemes, we find that the deviations between the full 3D model and the simplified 2D quantum-dot model are very significant. The full 3D model is found to reproduce the experimental data for a large class of QD structures where simplified 2D models fail. We conclude that this is due to the unphysical character of the pure 2D confinement, for which the various approximation schemes often yield unreliable results. A proper description of the QD structure in terms of fully 3D single-particle wave functions is therefore required; we have shown that in this case approximate approaches can give an accurate description of correlation effects in the macroatoms made available by present semiconductor technology.

ACKNOWLEDGMENTS

We are grateful to D. Pfannkuche and D. Vanossi for useful discussions. This work was supported in part by the EC through the TMR Network ''Ultrafast quantum optoelectronics,'' and by MURST–Italy.

APPENDIX A: CM AND RM SOLUTIONS FOR THE TWO-ELECTRON DOT

The present appendix is organized as follows: In Sec. A 1 we shall show how to reduce the 3D cylindrical helium problem to an effective two-dimensional one; in Sec. A 2 we shall summarize the 2D and 3D solutions of the one-particle Schrödinger equations for the center-of-mass and the relative-motion Hamiltonians, $\hat{H}_{\rm CM}$ and $\hat{H}_{\rm rm}$, as defined in Eqs. (11) and (12).

1. 3D eigenvalue equation for the cylindrical QD

If only the lowest single-particle state $\phi_0(z)$ of the quantum well is relevant to the two-electron motion, we can write the spatial-part $\Psi(\boldsymbol{r}_1;\boldsymbol{r}_2)$ of our helium wave function as

$$\Psi(\boldsymbol{r}_1;\boldsymbol{r}_2)=\psi(x_1,y_1;x_2,y_2)\,\phi_0(z_1)\,\phi_0(z_2). \tag{A1}$$

This approximation is well justified for most cases of interest. Indeed, for the typical QD structure used in the experimental investigation of addition spectra[2] (the quantum-well width $L=12$ nm, the barrier height $V_0=200$ meV), and the energy separation between the ground and first-excited states along z is 56 meV, about one order of magnitude larger than typical in-plane single-particle confinement energies.

Let us now consider the global Schrödinger equation corresponding to the exact helium Hamiltonian of Eq. (9):

$$\hat{\mathcal{H}}\Psi(\boldsymbol{r}_1;\boldsymbol{r}_2)=E\Psi(\boldsymbol{r}_1;\boldsymbol{r}_2); \tag{A2}$$

by substituting Eq. (A1), multiplying both sides by $\phi_0^*(z_1)\phi_0^*(z_2)$, and integrating over z_1, and z_2, we obtain

$$\left[2\varepsilon_0^z+\sum_{i=1}^{2}\hat{H}_0(i)+\frac{e^2}{\kappa}c(|\boldsymbol{r}_1-\boldsymbol{r}_2|)\right]\psi(\boldsymbol{r}_1;\boldsymbol{r}_2)=E\psi(\boldsymbol{r}_1;\boldsymbol{r}_2). \tag{A3}$$

The eigenvalue equation is then reduced to a 2D one, since $\boldsymbol{r}_i\equiv(x_i,y_i)$ and $c(r)=c(|\boldsymbol{r}_1-\boldsymbol{r}_2|)$ is an *effective* Coulomb potential, accounting for the geometry of the system:

$$c(r)=\int_{-\infty}^{+\infty}dz_1\int_{-\infty}^{+\infty}dz_2\,\frac{|\phi_0^*(z_1)|^2|\phi_0^*(z_2)|^2}{\sqrt{r^2+(z_1-z_2)^2}}. \tag{A4}$$

From now on we will drop the constant ground-state energy along z (ε_0^z). As a first step, we evaluate $c(r)$ by solving the quantum well eigenvalue problem (allowing for different values of the effective mass in the well and in the barrier). Then we numerically integrate Eq. (A4). It is easy to show analytically some important properties of $c(r)$, namely, that

$$0\leqslant rc(r)\leqslant 1,\quad \forall r, \tag{A5}$$

$$\lim_{r\to 0} rc(r)=0, \tag{A6}$$

$$\lim_{r\to \infty} rc(r)=1. \tag{A7}$$

These properties tell us that for large distances $r\,c(r)$ tends to the bare Coulomb potential, and that it is strongly reduced in the neighborhood of the origin, i.e., the more relevant space region in the computation of Coulomb and exchange integrals. Figure 9 shows such an effective Coulomb potential C multiplied by the dimensionless variable x (introduced below) as a function of x for different values of the quantum-well width: A monotonic behavior is apparent, going from the bare Coulomb-potential value in the zero-width limit (the function is constant and equal to 1), into progressively smaller values, toward the infinite-width case.

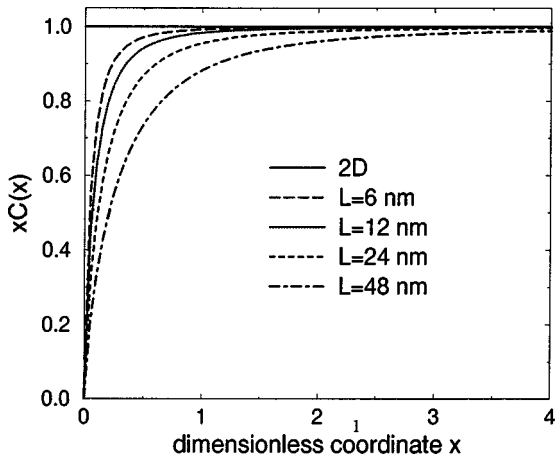

FIG. 9. Plot of the effective Coulomb potential $C(x)$ multiplied by the dimensionless coordinate $x\,[=x\,C(x)]$ as a function of x for different values of the quantum well width L and for a confinement energy $\hbar\omega_0=5$ meV. Notice that in the limit $L\to 0$ (2D case) $C(x)\to 1/x$ and, therefore, $x\,C(x)\to 1$.

2. Exact solutions

Let us first consider the CM equation, which has the form of a standard harmonic oscillator and can thus be solved analytically. For the 2D case (3D cylindrical), its eigenvalues are

$$\varepsilon^{2D}_{NM}=\hbar\omega_0(2N+|M|+1), \tag{A8}$$

$$N=0,1,2,\ldots,\quad M=0,\pm 1,\pm 2,\ldots,$$

and the corresponding orthonormalized eigenfunctions (the so called ''Fock-Darwin'' states[4,17]) are

$$\Phi^{2D}_{NM\sigma}(\boldsymbol{r},s)=\langle s,\boldsymbol{r}|NM\sigma\rangle=\lambda^{(|M|+1)/2}\sqrt{\frac{N!}{\pi(N+|M|)!}}e^{-iM\varphi}r^{|M|}e^{-(\lambda r^2/2)}L_N^{|M|}(\lambda r^2)\chi_\sigma(s). \tag{A9}$$

In the 3D spherical case,[18] the eigenvalues are

$$\varepsilon^{3D}_{NL}=\hbar\omega_0\left(2N+L+\frac{3}{2}\right),\quad N=0,1,2,\ldots,\quad L=0,1,2,\ldots, \tag{A10}$$

and the orthonormalized eigenfunctions $\Phi^{3D}_{NLM_z\sigma}(\boldsymbol{r},s)$ are

$$\Phi^{3D}_{NML_z\sigma}(\boldsymbol{r},s)=\langle s,\boldsymbol{r}|NLM_z\sigma\rangle=\sqrt{\frac{2\lambda^{L+3/2}N!}{\Gamma\left(N+Ł+\frac{3}{2}\right)}}r^Le^{-(\lambda r^2/2)}L_N^{L+1/2}(\lambda r^2)Y_{LM_z}(\vartheta,\varphi)\chi_\sigma(s). \tag{A11}$$

Here, $\lambda=m^*\omega_0/\hbar$, L_N^p are generalized Laguerre polynomials,[19] Γ is the usual gamma function, χ_σ denotes the spin function, and Y_{LM_z} are the spherical harmonics. We have used polar coordinates throughout: $\boldsymbol{r}\equiv(r,\varphi)$ in the 2D (3D cylindrical) case and $\boldsymbol{r}\equiv(r,\vartheta,\varphi)$ in the 3D spherical case. For the 2D (3D cylindrical) case the quantum numbers are (N,M,σ): N is the radial quantum number, M the angular momentum quantum number (in this case the total angular momentum coincides with the component along z, $L_z=-\hbar M$), and σ the spin component along z. In the 3D spherical case, on the other hand, the quantum numbers are given by (N,L,M_z,σ): here L is the total angular momentum quantum number, and M_z is the magnetic quantum number, $M_z=-L,-L+1,\ldots,L$.

Let us now come to the single-particle Schrödinger equation for the rm Hamiltonian of Eq. (12). In this equation the variables are easily separable, and the problem is reduced to the solution of a radial differential equation. For the 2D (3D cylindrical) case, the rm eigenfunction in coordinate space is

$$\varphi_{nm}(\boldsymbol{r})=R_{nm}(r)\frac{e^{-im\varphi}}{\sqrt{2\pi}}, \tag{A12}$$

where $R_{nm}(r)$ is the solution of the radial Schrödinger equation

$$\frac{\partial^2 R_{nm}(r)}{\partial r^2}+\frac{1}{r}\frac{\partial R_{nm}(r)}{\partial r}+\left[k_{nm}^2-\tilde{\lambda}^2 r^2-\alpha c(r)-\frac{m^2}{r^2}\right]R_{nm}(r)=0; \tag{A13}$$

we have employed the notations $\tilde{\lambda}=\mu\omega_0/\hbar, \alpha=2\mu e^2/\kappa\hbar^2$, and $k_{nm}^2=2\mu\epsilon_{nm}/\hbar^2$, where ϵ_{nm} is the rm eigenvalue. The effective Coulomb potential $c(r)$ is simply $1/r$ in the 2D case, and it is defined in Sec. A 1 for the 3D cylindrical case.

For the 3D spherical case, the rm eigenfunction in coordinate space is

$$\varphi_{nlm_z}(\boldsymbol{r})=R_{nl}(r)Y_{lm_z}(\vartheta,\varphi), \tag{A14}$$

with $R_{nl}(r)$ satisfying the radial eigenvalue equation

$$\frac{\partial^2 R_{nl}(r)}{\partial r^2}+\frac{2}{r}\frac{\partial R_{nl}(r)}{\partial r}+\left[k_{nl}^2-\tilde{\lambda}^2 r^2-\frac{\alpha}{r}-\frac{l(l+1)}{r^2}\right]R_{nl}(r)=0; \tag{A15}$$

where, again, we put $k_{nl}^2=2\mu\epsilon_{nl}/\hbar^2$, and ϵ_{nl} is the rm eigenvalue.

In order to obtain an exact solution for the rm eigenvalue problems, we rewrite Eqs. (A13) and (A15) in terms of the dimensionless variable $x=\tilde{\lambda}^{1/2}r$. For the 2D (3D cylindrical) case, Eq. (A13) becomes

$$\begin{gathered}\frac{d}{dx}\left(x\frac{d\tilde{R}_{nm}(x)}{dx}\right)+\left[-\frac{m^2}{x}-\tilde{\alpha}\,x\,C(x)+\tilde{k}_{nm}^2 x-x^3\right]\tilde{R}_{nm}(x)=0,\\ \tilde{R}_{nm}(x)=R_{nm}(r),\\ C(x)=\tilde{\lambda}^{-1/2}c(\tilde{\lambda}^{-1/2}x)\end{gathered} \tag{A16}$$

[for the 2D case it is simply $C(x)=1/x$], while for the 3D case Eq. (A15) transforms into

$$\begin{gathered}\frac{d^2\tilde{\chi}_{nl}(x)}{dx^2}+\left[-\frac{l(l+1)}{x^2}-\frac{\tilde{\alpha}}{x}+\tilde{k}_{nl}^2-x^2\right]\tilde{\chi}_{nl}(x)=0,\\ \tilde{\chi}_{nl}(x)=\chi_{nl}(r), \quad \chi_{nl}(r)=\frac{R_{nl}(r)}{r}.\end{gathered} \tag{A17}$$

The dimensionless parameters are $\tilde{\alpha}=\tilde{\lambda}^{-1/2}\alpha=2\sqrt{\mathcal{R}^*/\hbar\omega_0}$ and $\tilde{k}_\alpha^2=k_\alpha^2/\tilde{\lambda}=2\epsilon_\alpha/\hbar\omega; \mathcal{R}^*=e^4m^*/2\kappa^2\hbar^2$ is the effective Rydberg energy. Actually, exact analytic solutions exist, but they are limited to 2D and 3D spherical cases only[20,21]; thus we have chosen to solve Eqs. (A16) and (A17) by standard numerical methods. We stress that the numerical accuracy depends on the accurate specification of the boundary conditions that we impose through analytical asymptotic formulas for eigenfunctions near to the singular points 0 and $+\infty$, following the general methods of Ref. 22. In this way the numerical solution is very stable and efficient, thus overcoming possible difficulties related to the singlet ground state[7]; in our calculations energy values are obtained with a nominal relative error of the order of 10^{-8}.

APPENDIX B: HELIUM PERTURBATION THEORY

We employ the standard Rayleigh-Schrödinger perturbation theory to correct the SSH eigenvalues in Eq. (18) at the second order in the off-diagonal Coulomb matrix elements entering the total Hamiltonian (17). In the remaining part of this section we shall consider the 2D and 3D spherical cases, by neglecting the center-of-mass motion.

For the 2D case, the rm SSH eigenvalues $\epsilon_{nm}^{\mathrm{SSH}}$ are given by[10]

$$\epsilon_{nm}^{\mathrm{SSH}}=\hbar\omega_0(2n+|m|+1)+\sqrt{\mathcal{R}^*\hbar\omega_0}\,S^{2D}(n,m), \tag{B1}$$

$$S^{2D}(n,m)=\frac{\Gamma\left(|m|+\frac{1}{2}\right)}{|m|!}\left\{1+\sum_{s=0}^{n-1}\frac{n!(-1)^{s+1}[(2s+1)!!]^2|m|!}{(n-s-1)!\,2^{2s+2}[(s+1)!]^2(|m|+s+1)!}\right\}, \tag{B2}$$

while for the 3D case we have

$$\epsilon_{nl}^{\mathrm{SSH}}=\hbar\omega_0\left(2n+l+\frac{3}{2}\right)+\sqrt{\mathcal{R}^*\hbar\omega_0}\;S^{3D}(n,l), \tag{B3}$$

$$S^{3D}(n,l)=\frac{l!\,\Gamma\left(\frac{1}{2}\right)(2l+1)!!}{2^{l+1}\Gamma^2\left(l+\frac{3}{2}\right)}\left\{1+\sum_{s=0}^{n-1}\frac{n!(-1)^{s+1}\Gamma\left(\frac{1}{2}\right)[(2s+1)!!]^2(2l+1)!!}{2^{s+l+3}(n-s-1)!\,\Gamma\left(s+l+\frac{5}{2}\right)[(s+1)!]^2}\right\}. \tag{B4}$$

The first-order correction due to nondiagonal Coulomb matrix elements is equal to zero. The second-order correction $\Delta\varepsilon_0^{(2)}$ to the ground-state energy is given by the well-known expression

$$\Delta\varepsilon_0^{(2)}=\sum_n \frac{|V_{0n}|^2}{\varepsilon_0^{\mathrm{SSH}}-\varepsilon_n^{\mathrm{SSH}}} \tag{B5}$$

[see the notation in Eq. (17)]. The idea now is to look for analytic expressions for the off-diagonal integrals V_{0n} and then to perform a numerical summation. However, expressions like those obtained in Eqs. (B2)–(B4) (Ref. 23) are not useful, since each integral is given by an alternated-sign summation, and numerical errors become rapidly critical as the quantum number n increases. In contrast, the solution can be obtained using an integration trick suggested in Ref. 24, so that all the terms in the summation are obtained with the same sign. For the 2D case one obtains

$$V_{n0}=\sqrt{\mathcal{R}^*\hbar\omega_0}\,\frac{\Gamma\left(n+\frac{1}{2}\right)}{\Gamma(n+1)},$$

$$V_{n0}\approx\sqrt{\mathcal{R}^*\hbar\omega_0}\,\frac{1}{n^{1/2}},\quad n\to\infty. \tag{B6}$$

For the 3D case one obtains

$$V_{n0}=\sqrt{\mathcal{R}^*\hbar\omega_0}\,\sqrt{\frac{\Gamma^2\left(n+\frac{1}{2}\right)}{\pi\,\Gamma(n+1)\,\Gamma\left(n+\frac{3}{2}\right)\Gamma\left(\frac{3}{2}\right)}},$$

$$V_{n0}\approx\sqrt{\mathcal{R}^*\hbar\omega_0}\,\frac{1}{\sqrt{\pi\,\Gamma\left(\frac{3}{2}\right)}}\,\frac{1}{n^{3/4}},\quad n\to\infty. \tag{B7}$$

As already pointed out, now the generic terms (B6) and (B7) in the sum (B5) have the same sign and the summation can be easily performed. The result for the 2D case is

$$\Delta\varepsilon_0^{(2)}=-\mathcal{R}^*\ (0.691), \tag{B8}$$

and for the 3D case it is

$$\Delta\varepsilon_0^{(2)}=-\mathcal{R}^*\ (0.156). \tag{B9}$$

Note that the 3D term is significantly smaller than the corresponding 2D one, and that in the 3D case the series converges more quickly.

[1] For recent reviews, see R. C. Ashoori, Nature (London) **379**, 413 (1996); L. P. Kouwenhoven, C. M. Marcus, P. L. McEuen, S. Tarucha, R. M. Westervelt, and N. S. Wingreen, in *Mesoscopic Electron Transport*, edited by L. L. Sohn, L. P. Kouwenhoven, and G. Schoen (Kluwer, Dordrecht, 1997), p. 105.

[2] S. Tarucha, D. G. Austing, T. Honda, R. J. van der Hage, and L. P. Kouwenhoven, Phys. Rev. Lett. **77**, 3613 (1996).

[3] M. Fricke, A. Lorke, J. P. Kotthaus, G. Medeiros-Ribeiro, and P. M. Petroff, Europhys. Lett. **36**, 197 (1996).

[4] For a recent review, see L. Jacak, P. Hawrylak, and A. Wójs, *Quantum Dots* (Springer, Berlin, 1998); see also N. F. Johnson and M. Reina, J. Phys.: Condens. Matter **4**, L623 (1992); J. J. Palacios, L. Martin-Moreno, G. Chiappe, E. Louis, and C. Tejedor, Phys. Rev. B **50**, 5760 (1994), and references therein.

[5] M. Rontani, F. Rossi, F. Manghi, and E. Molinari, Appl. Phys. Lett. **72**, 957 (1998).

[6] A few examples of 3D calculations exist in the literature; see, e.g., Y. Tanaka and H. Akera, Phys. Rev. B **53**, 3901 (1996); A. Wojs, P. Hawrylak, S. Fafard, and L. Jacak, *ibid.* **54**, 5604 (1996); T. Ezaki, N. Mori, and C. Hamaguchi, *ibid.* **56**, 6428 (1997).

[7] D. Pfannkuche, V. Gudmundsson, and P. A. Maksym, Phys. Rev. B **47**, 2244 (1993).

[8] J. Hubbard, Proc. R. Soc. London, Ser. A **276**, 238 (1963).

[9] These are the so-called Roothaan equations: see, e.g., I. Levine, *Quantum Chemistry* (Prentice-Hall, Englewood Cliffs, NJ, 1991). For applications to 2D quantum dots, see Refs. 7 and 11.

[10] U. Merkt, J. Huser, and M. Wagner, Phys. Rev. B **43**, 7320 (1991).

[11] L. Wang, J. K. Zhang, and A. R. Bishop, Phys. Rev. Lett. **73**, 585 (1994).

[12] A. Wójs and P. Hawrylak, Phys. Rev. B **53**, 10 841 (1996).

[13] M. Koskinen, M. Manninen, and S. M. Reimann, Phys. Rev. Lett. **79**, 1389 (1997).

[14] Since in these cases the energy balance defining the ground-state energy according to Eq. (8) becomes very delicate, the dependence of Coulomb and exchange integrals on the dot dimensionality may give rise to different ground-state spin polarizations in 2D and 3D QD's.

[15] A. Kumar, S. E. Laux, and F. Stern, Phys. Rev. B **42**, 5166 (1990).

[16] C. Steinebach, C. Schüller, G. Biese, D. Heitmann, and K. Eberl, Phys. Rev. B **57**, 1703 (1998).

[17] V. Fock, Z. Phys. **47**, 446 (1928).

[18] S. Flügge, *Practical Quantum Mechanics* (Springer-Verlag, Berlin, 1971).

[19] *Handbook of Mathematical Functions*, edited by M. Abramowitz and I. A. Stegun (Dover, New York, 1972).
[20] M. Taut, Phys. Rev. A **48**, 3561 (1993).
[21] M. Dineykhan and R. G. Nazmitdinov, Phys. Rev. B **55**, 13 707 (1997). This paper also considers different in-plane and orthogonal single-particle parabolic confinement potentials.
[22] P. Moon and D. E. Spencer, *Field Theory Handbook* (Springer-Verlag, Berlin, 1961).
[23] A. Wójs and P. Hawrylak, Phys. Rev. B **51**, 10 880 (1995); E. Anisimovas and A. Matulis, J. Phys.: Condens. Matter **10**, 601 (1998).
[24] M. Stone, H. W. Wyld, and R. L. Schult, Phys. Rev. B **45**, 14 156 (1992).